First direct proof of internal conversion between bound states

T. Carreyre,[1] M. R. Harston,[2] M. Aiche,[1] F. Bourgine,[1] J. F. Chemin,[1] G. Claverie,[1] J. P. Goudour,[1] J. N. Scheurer,[1] F. Attallah,[3] G. Bogaert,[4] J. Kiener,[4] A. Lefebvre,[4] J. Durell,[5] J. P. Grandin,[6] W. E. Meyerhof,[7] and W. Phillips[5]
[1]*Centre d'Etudes Nucléaires de Bordeaux-Gradignan, F-33175 Gradignan, France*
[2]*Service de Physique Nucléaire, DSM/DAPNIA, CEA, F-91191 Gif sur Yvette, France*
[3]*Gesellschaft für Schwerionenforschung (GSI), D-6100 Darmstadt, Germany*
[4]*Centre de Spectroscopie Nucléaire et de Spectrométrie de Masse, F-91405 Orsay-campus, France*
[5]*University of Manchester, Manchester, United Kingdom*
[6]*Centre Interdisciplinaire de Recherches avec des Ions Lourds, CEA-CNRS, BP 5133, F-14040 Caen, France*
[7]*Stanford University, Department of Physics, Stanford, California 94305-4060*
(Received 14 January 2000; published 19 July 2000)

We present direct evidence for the process of internal conversion between bound atomic states (BIC) when the binding energy of the converted electron becomes larger than the nuclear transition energy. This process has been proposed as an explanation of the measured, unexpectedly short lifetime of the first excited state of ^{125}Te with charge state larger than 44^+. We have detected the K_α x rays emitted in flight which follow the filling of the *K*-shell vacancy created by the bound internal conversion process, together with γ rays from Te ions in charge states ranging between 44^+ and 48^+. For Te^{45+} and Te^{46+}, the comparison of the x-ray to γ-ray ratios with the theoretical calculations of the internal conversion coefficients including decay to bound atomic states, assuming Te ions in their ground electronic state, show poor agreement. The agreement becomes good if account is taken of BIC decay of excited initial states with different occupancies of the $2p_{1/2}$ and $2p_{3/2}$ subshells. In this situation, the half-life becomes sensitive to the precise initial state and simple specification of the charge state alone is no longer appropriate.

PACS number(s): 23.20.Nx, 21.10.Tg, 27.60.+j

INTRODUCTION

Previous reports [1,2] have shown that in highly ionized ^{125}Te, the lifetime of the first excited nuclear state at 35.4919 $\pm$0.0005 keV depends strongly on the ionic charge state of the Te ion in the charge state range between 44^+ and 48^+. A large increase of the lifetime found for charge states 47^+ and 48^+ was explained by the blocking of the *K*-shell internal conversion (IC) because the binding energy of a *K*-shell electron for these charge states becomes larger than the excitation energy of the nuclear state E_γ. The increase of the *K*-shell binding energy (E_{1s}) is due to the reduction in the screening of the Coulomb nuclear potential by the outer shell electrons.

Rather surprisingly, for the charge states 45^+ and 46^+, the lifetime of the level was found to have a value close to that in the neutral atom. For these two charge states, an increase of the lifetime was expected since the condition $E_{1s} > E_\gamma$ is fulfilled. It was suggested in Ref. [1] that the nuclear transition could still be converted, but without the emission of the electron into the continuum, the electron being promoted from the *K* shell to another bound state lying close to the continuum. It was argued that, because the density of states just below the limit of the energy continuum is high, and because the atomic width associated with the hole in the $1s$ state is as large as a few eV, it is highly probable to find a transition that matches the nuclear transition energy, allowing a type of internal conversion to take place. This new process, called bound internal conversion (BIC), bears the same relationship to the usual IC process, as electronic excitation does to ionization [3].

One important feature of BIC is its stongly resonant character. Thus, a change of a few eV in the atomic excitation energy can result in a large variation in the nuclear decay rate and nuclear half-life. In particular cases such as highly charged ions, where the matching of atomic and nuclear excitation energies can be achieved at the level of eV, the value of the half-life $T_{1/2}$ can be significantly smaller than in the neutral atom. The dependence of the lifetime on the associated charge state and atomic configuration may have important consequences in astrophysical plasmas as discussed previously in the framework of β^- decay in highly charged ions [4,5]. In principle, BIC can play an important role in cases where the binding energies of the atomic electrons are close to the nuclear transition energy. For the particular case of electronic transitions from the *K* shell and transitions connecting one excited state to the ground nuclear state, this situation is encountered in several nuclei in addition to ^{125}Te (such as ^{191}Ir, ^{196}Au, ^{183}Ta, ^{177}Ta, ^{187}Os). Many more cases can be found if transitions between excited states are considered.

In this paper, we report the results of an experiment which is a direct proof of the existence of BIC. The signature of BIC is the observation of the delayed K_α x rays following the filling of the *K*-shell vacancy produced by the internal conversion of the nuclear transition. In the first part of the paper, we describe the experimental method. Then we compare the experimental photon spectra with the results of simulations assuming a single internal conversion coefficient and one unique nuclear lifetime for any particular charge state as suggested in Ref. [6]. Finally, the results are compared with a new set of calculations for an internal conversion coefficient which takes into account the possible excita-

tion of electrons inside the $2p$ shell at the time of nuclear decay [7].

EXPERIMENTAL SETUP

The experiment was performed at GANIL. A beam of 25 MeV/nucleon of ^{125}Te ions in the charge state 38^+ impinged on a 1 mg/cm^2 thick ^{232}Th target in order to strip the ions and to Coulomb excite the Te nuclei. The beam intensity was of the order of 1 enA. The Te ions exiting from the target had an approximately Gaussian charge distribution centered on $\langle Q \rangle = 46.5$ with standard deviation $\sigma_Q = 1.6$ (see Ref. [2]). Scattered Te ions with $Q = 44-48$ within the angular range $\theta_{\text{coulex}} = 1-6°$ were accepted in the SPEG [8] spectrometer, which was rotated to a mean angle of 3.5°.

The distance between the beam focal point on the target and the entrance of the first dipole of SPEG was 3 m. The corresponding time of flight of the ions from the target to the spectrometer was 40 ns, allowing for atomic and nuclear decay before entering the magnetic field. The Te ions were then separated in the magnetic field of SPEG according to their charge state. At the exit of the separation system, the horizontal (X) and vertical (Y) positions of the ^{125}Te ions were detected event by event in two identical drift chambers, separated by a distance of 1.58 m. From these parameters, the distributions in horizontal angle, θ, and vertical angle, ϕ, of ^{125}Te ions entering the detection system were calculated. The coincidence signal between a parallel plate avalanche counter and the cyclotron high frequency provided a fast trigger signal for the data acquisition system.

The energy of the scattered ions was measured in an ionization chamber located downstream of the drift chambers. The ionization chamber consisted of eight elements, the first two of which were used to measure the differential energy loss, thereby allowing a selection of atomic numbers of the reaction products.

In the passage through the target, nuclear and atomic excitation of the Te beam were induced. In the range of scattering angles analyzed by SPEG, below the grazing angle at 6.6°, nuclear Coulomb excitation was the dominant mechanism for the excitation of the Te nuclei. A fraction of ^{125}Te nuclei were Coulomb excited to high spin, short-lived states which populate the first excited, $J = 3/2^+$ state of ^{125}Te at 35.492 keV. In the neutral atom, this state has a half-life of $T^0_{1/2} = 1.486$ ns. The decay in-flight of this state by γ-ray emission or by internal conversion with subsequent emission of Te K x rays, referred to hereafter as IC x rays, was detected by an array of four 10-cm^2 planar Ge detectors described further below.

Pure atomic collisions between the beam and the Th target atoms induced vacancies in the Te K shell which were filled promptly with emission of Te K x rays. As far as the excitation of the Te K shell is concerned, the collisions at this energy are in the quasimolecular regime [9]. Te K vacancies are formed by excitation of the $2p\sigma$ molecular orbital due to the time-varying Coulomb potential acting on the electron. From an extrapolation of the results for Xe + Th collisions at 5.9 MeV/nucleon [10], a 300 b cross section for the production of Te K x rays was estimated, using the scaling laws developed by Anholt *et al.* [10].

The lifetime of the K shell vacancies in Te ions with a half-filled L shell is of the order of 10^{-16} s [11]. The K vacancies created in the Te ions at the end of the collision are filled by $2p$ electrons within 100 μm behind the target with emission of K x rays, the energies of which depend on the charge state and electronic configuration. In Te^{46+} the calculated K x-ray energy is approximately 28.1 keV.

The other collision partner Th is more likely to undergo direct ionization of the L shell. The scaling laws applied to the Xe +Th collision system yield an ionization probability of the order of unity, so in each collision one L shell vacancy should be formed. In the following, we refer to x rays produced in pure atomic collisions as atomic x rays (AT x rays).

Two Ge detectors were mounted in the horizontal plane at 135° with respect to the beam direction and two other Ge detectors were placed at 45° out of the horizontal plane at a mean angle of 120° with respect to the beam direction. The energy resolution of the detectors was 700 eV at 30 keV. The fast and slow output signals from the Ge detectors were recorded in coincidence with the signals issued from the ion detection system.

In order to optimize the discrimination between K x rays emitted in the decay of the nuclear state with a mean delay of the order of the nuclear half-life and the Te K x rays following the filling of K shell vacancies created in atomic collisions, the target was surrounded by lead and copper shielding so that the Ge detectors viewed a zone along the beam located at a mean distance of 8.7 cm behind the target. Therefore, only the delayed Te K x rays following the IC process and γ rays at 35.49 keV, were expected to reach the detectors. These two radiations, emitted from Te ions in flight and detected in the backward direction at approximately 120° undergo a large Doppler effect ($v/c = 0.227$), which induces a negative energy shift, lowering the mean energies of the Te IC K x rays and the γ rays to 24 and 29.6 keV, respectively.

In spite of the shielding, prompt (AT) x rays emitted at the target position can reach the detectors if they are emitted in a forward direction, through the beam aperture in the shielding material surrounding the target, and then are scattered in the direction of the detectors. The Doppler shift associated with these AT Te K x rays is positive and leads to a maximum energy for AT Te K x rays equal to 34.3 keV. Hence, the Doppler effect enables a discrimination between the two different mechanisms producing Te K x rays in the collision. Most AT Th L x rays are emitted from atoms with a small recoil velocity, so that their x-ray energy is much less affected by the Doppler effect.

The Ge spectra from the four detectors were gain-matched off-line and added together. The different sources of background in the Ge spectrum are discussed in the next paragraph.

DATA ANALYSIS AND RESULTS

The data analysis follows closely the procedure described in Ref. [2]. However, in contrast to the experiment of Ref. [2], the charge state remained unaltered in the spectrometer

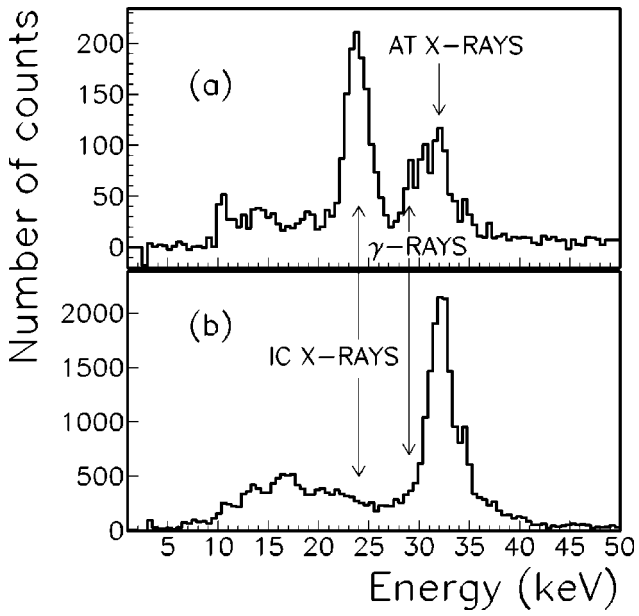

FIG. 1. Experimental photon spectra in coincidence with Te ions in charge states ranging between 44^+ and 48^+. Spectrum (a) is gated by the inelastic contour, see text and Fig. 2. Spectrum (b) is gated by the elastic contour, see text and Fig 2. The positions of AT x rays, IC x rays, and γ rays are indicated by arrows.

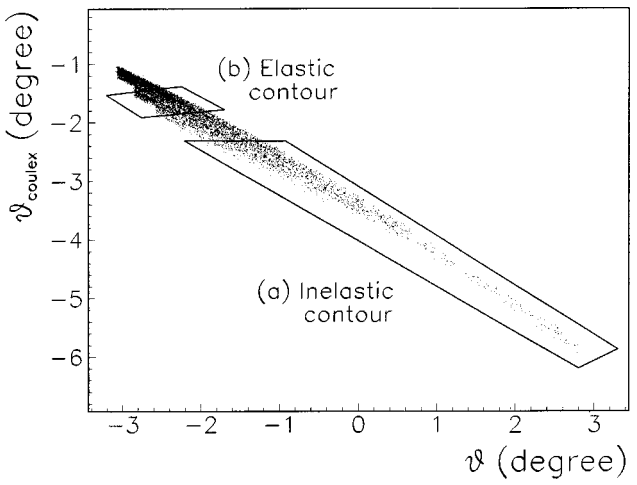

FIG. 2. Bidimensional plot of the scattering angle in the target θ_{coulex} versus the angle at the exit of the last quadrupole θ given by the TURTLE+ simulation. The inelastic contour (a) and the elastic contour (b) are used for conditioning experimental and simulated spectra.

because the 3 m distance between the target and the entrance of the magnetic field was large enough to allow for the decay of the nuclear excited ^{125}Te to take place before the ion entered SPEG.

Different bidimensional matrices of events were sorted from the raw data set. A contour in the bidimensional plot giving the energy of the ions in the ionization chamber versus the X position in the first drift chamber was chosen to reduce the background associated with energy degraded events. Different X positions selected different charge states. For each event in this contour, the angle of emergence from the last quadrupole θ was then calculated from the horizontal positions $X1$ and $X2$ in the two drift chambers. As shown in the next section, the angular distribution in θ reflects the corresponding contribution of Te scattering angles θ_{coulex} in the target.

Random events in the Ge spectrum were subtracted from the true plus random events by setting contours in the bidimensional matrix of the photon energy versus delay time between the PPAC and fast Ge discriminator output signals. Finally, Ge spectra of true events were obtained for each Te charge state between 44^+ and 48^+.

Because a maximum of four charge states could be recorded at one magnetic rigidity in the focal plane of SPEG, we used two consecutive values of the magnetic rigidity in order to analyze Te charge states ranging from 44^+ to 48^+. The values of the rigidity were chosen to bring successively the 46^+ and 47^+ charge states to the center of the drift chambers. The final Ge spectrum for a given charge state was obtained by summing the spectrum for each rigidity.

Ge energy spectra corresponding to the sum of the spectra for all charge states, are shown in Fig. 1. Spectra (a) and (b) are conditioned by contours set on the scattering angles corresponding to θ_{coulex} between 2.3° and 6° and between 1.3° and 1.9° degrees, respectively. In the following, the events selected by these two contours, shown in Fig. 2, are referred to as inelastic and elastic, respectively.

Below 10 keV, the cut in each spectrum was due to the energy discrimination thresholds. Between 10 and 50 keV, the different kinds of radiation in each spectrum can be identified. The flat high energy background is due to Compton scattering from high-energy γ rays in the detectors and in the material surrounding the target. These γ rays are mainly produced by the deexcitation of Coulomb-excited nuclear states of projectile and target.

Characteristic lines between 10 and 20 keV correspond to target L x rays rescattered in the direction of the detectors. Since the recoil velocity of the Th atoms is small, the lines are not Doppler shifted, but they are broadened strongly by the formation of multiple vacancies in the Th atomic shells.

The line at 31.8 keV is due to AT x rays, following the direct Coulomb ionization of the projectiles in the target, emitted in the forward direction with a maximum Doppler shift and then scattered by the surrounding materials in the direction of the detectors. This line dominates in the spectrum (b) associated with the elastic contour for which the nuclear excitation is strongly suppressed. We find that the relative intensity of this Te component remains independent of the ionic charge state.

The line at 24 keV corresponds to IC Te K x rays emitted in the backward direction, at around 130°. This line is not seen in spectrum (b) which is associated with large impact parameter collisions and a small nuclear excitation probability. On the other hand, this line dominates spectrum (a), reflecting the strong dependence of the Coulomb excitation probability of the nucleus on the scattering angle. The intensity of this line is strongly dependent on the Te charge state. The γ transition at 35.49 keV, competing with the IC decay, is also seen in spectrum (a) doppler shifted to an energy of

29.6 keV. This line appears as a shoulder on the low-energy side of the 31.8-keV line.

SIMULATIONS

For a quantitative interpretation of the results we performed two different simulations. One, for the analysis of the ion trajectories in the spectrometer, was made with the program TURTLE+ [12]. The second used the program GEANT [13] for the analysis of Ge spectra. The GEANT simulation takes into account Compton and elastic scattering of all radiations in the shielding and chamber materials. The parameters entering the trajectory analysis were (i) the beam dispersion parameters $\delta\theta$, $\delta\phi$, $\delta p/p$ (p=ion momentum); (ii) the magnetic rigidity; (iii) the scattering angle θ_{coulex}; (iv) the target thickness; (v) the experimental yield of charge state.

In Fig. 2, we show the bidimensional plot of θ_{coulex} versus the angle of emergence from the last quadrupole θ. The contours used to select the Ge spectra associated with elastically and inelastically scattered Te are shown.

The parameters entering in the simulation of the Ge spectra by the program GEANT were (i) the geometry of the reaction chamber, including the shielding of the detectors; (ii) the energy resolution of the Ge detectors; (iii) the beam energy and beam angular distributions at the exit of the target; (iv) the experimental yield of charge states; (v) the production of atomic Te K and Th L x rays at the target; (vi) the angle-dependent nuclear Coulomb excitation probability of Te nuclei $P(\theta_{\text{coulex}})$ and subsequent probability feeding of the first excited state of ^{125}Te; (vii) the production of high-energy γ rays from the decay of high spin states of ^{125}Te; (viii) the energy dependence of the $2p$-$1s$ transition on the Te charge state; (ix) the time-dependent rate of the in-flight decay of the first excited state of ^{125}Te nuclei by internal conversion in the L and K shells and by γ emission. We performed separate simulations for each type of radiative process, namely, high-energy γ emission, AT Te K and Th L x-ray emission, starting with the same number of events for each type of process. The cross sections for these processes were assumed to be independent of the Te charge state.

Next, we simulated the Ge spectra for the decay of the first excited nuclear state by γ emission or IC followed by emission of a Te K x ray. In the neutral Te atom, Auger transitions associated with $2s$ and $2p$ electrons contribute to 8% of the K hole width [14]. Measurements of the K-shell fluorescence yield in highly ionized ions of Fe indicate that the Auger contribution remains of the same order in carbonlike and nitrogenlike ions as in the neutral atom [15]. In consequence, IC followed by an Auger process were neglected in the simulation.

Following the analysis of the previous experiment [1,2], we assumed first that Te ions at the exit of the target are in the ground electronic state for each charge state Q. Then a single value of the internal conversion coefficients α_K^Q and α_L^Q and consequently a single value $T_{1/2}^0$ is inferred for each charge state Q of the Te ions. The total IC coefficient α_T^Q is given by

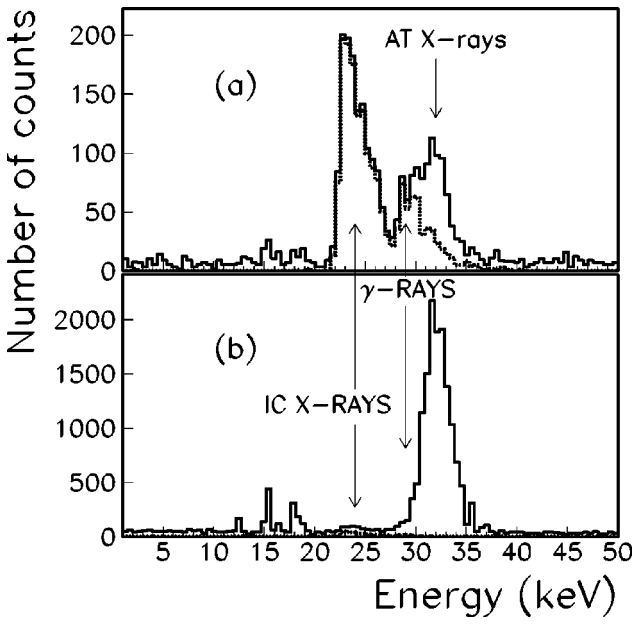

FIG. 3. In flight decay photon spectra simulated with the GEANT code. The charge states of the Te ions and the angular contours are the same as for Figs. 1 and 2. The value of $T_{1/2}$ from Refs. [1,2] and reported in Table I column 6 are used in the simulation. In the inelastic spectrum (a) and in the elastic spectrum (b), the spectrum arising from IC x rays and γ rays is shown by dotted-dashed lines. The thick solid lines give the total simulated spectra including the contribution of AT x rays from Te and Th.

$$\alpha_T^Q = \alpha_K^Q + \alpha_L^Q . \tag{1}$$

The values for α_L^Q were computed using the standard methods for normal internal conversion [6].

The Q-dependent α_T^Q is related to the Q dependence of the half-life of the nuclear state, $T_{1/2}^Q$ by the relation

$$T_{1/2}^Q = T_{1/2}^0 (1+\alpha_T^0)/(1+\alpha_T^Q), \tag{2}$$

where $\alpha_T^0 = 13.91$ and $T_{1/2}^0 = 1.486$ ns are, respectively, the IC coefficient and the half-life in the neutral atom. The simulations cover a range of half-lives of the first excited nuclear state of ^{125}Te ions $T_{1/2}$ between 0.7 and 10 ns. For each value $T_{1/2}^Q$, the value of α_T^Q in the simulation was changed according to Eq. (2). The location of the decaying ion drifting between the target and SPEG, was randomly sampled from an exponential decay law.

The scattering angles were distributed between 1.3° and 6° according to the Rutherford scattering law. The number of excited ^{125}Te nuclei was obtained from the theoretical values for $P(\theta_{\text{coulex}})$. The results of the simulations were stored event by event in order to obtain the Ge energy spectrum associated with the scattering angle for each ionic species. Finally the simulated Ge spectrum for the different decay processes were scaled and added together.

We show in Fig. 3 the result of a simulation using the values of $T_{1/2}$ given by Attallah *et al.* [1,2] and reported in Table I. As in Fig. 1, the spectra (a) and (b) correspond to inelastic and elastic scattering, respectively. It is seen that the

TABLE I. Measured and calculated internal conversion coefficients and half-lives of the first excited state of Te^{125}.

Charge state	α_K Exp.[a]	α_K Exp.[b]	α_K Calc.[c]	$T_{1/2}$ (ns) Exp.[a]	$T_{1/2}$ (ns) Exp.[b]	$T_{1/2}$ (ns) Calc.[c]
44	$\geqslant 8$		10.8	$\leqslant 2$		1.6
45	$13^{+6}_{-3.5}$	$\geqslant 11$	5.9	$1.4^{+0.4}_{-0.4}$	$\leqslant 1.5$	2.6
46	$\leqslant 19, \geqslant 2.8$	10 ± 2	0.6	$\leqslant 4, \geqslant 1$	1.8 ± 0.4	6.7
47	$\leqslant 0.6$	1.1 ± 0.5	0.2	$\geqslant 7$	6 ± 1	7.9
48	$\leqslant 0.5$			$\geqslant 9$	11 ± 2	10.1

[a]Present experiment.
[b]Reference [2].
[c]Reference [6].

experimental spectra in Fig. 1 and the simulated spectra in Fig. 3 are in good qualitative agreement. This comparison shows that all the relevant processes involved in the photon emission have been included in the simulation. In Fig. 3, the contribution of the nuclear decay of the first excited state of Te by IC and by γ emission is indicated by a dotted line.

DISCUSSION OF THE RESULTS

In Figs. 4(a)–4(d) we show the experimental Ge spectra conditioned by the inelastic contour on θ_{coulex}, and by the charge state of the detected Te ions equal to 44^+, 45^+, 46^+, and 47^+, respectively. For each spectrum, we have subtracted the corresponding spectrum conditioned by the elastic contour after normalization on the number of Te ions. The spectra in Figs. 4(e)–4(h) correspond to simulation of the Ge spectra for the nuclear decay of Te alone. These spectra are conditioned by the charge state after magnetic analysis and by the inelastic contour as for the corresponding experimental spectra in Figs. 4(a)–4(d).

Varying step by step, the value of $T_{1/2}$ in the simulation, we have calculated for each spectrum the ratio $\rho = N_{\text{IC}}/N_\gamma$, of the number of IC x rays in the energy interval 21.5 to 25.5 keV, N_{IC}, to the number of of γ rays in the energy interval 28.0 to 32.5 keV, N_γ. From each experimental spectrum of a given charge state, we have extracted a ρ^Q value. This ρ^Q value was then compared with the curve ρ versus $T_{1/2}$ obtained from the simulation in order to determine the best estimate of $T_{1/2}$ or, from Eqs. (1) and (2) , the best value of α_T^Q and α_K^Q. The spectra in Figs. 4(e)–4(h) assume these particular values.

Te^{44+}. Starting the analysis with the spectrum in Fig. 4(a) gated by Te ions detected in the charge state $Q=44$, we note the presence of a Te K x-ray peak at 24 keV, signaling IC decay. In this case, IC, followed by the emission of an electron in the continuum induces a change of the charge state of the Te ion by one unit. The x-ray signal detected in coincidence with charge $Q=44$ corresponds to IC in a Te nucleus with ionic charge state $Q=43$. The number of ions produced in this charge state which also contribute to the x-ray signal in the photon spectrum in Fig. 4(a) is low because of the charge state distribution of ions at the exit of the target. The γ signal at 29 keV is in coincidence with Te^{44+}.

In the simulation, the decays of Te^{43+} and Te^{44+} were

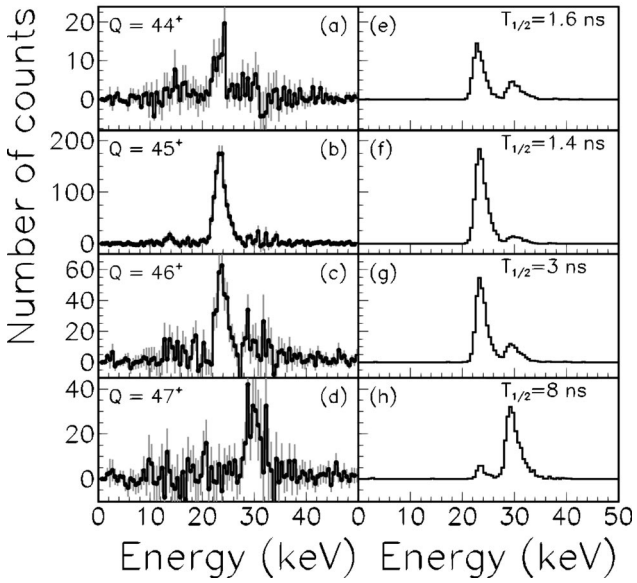

FIG. 4. (a) Spectra of IC x rays and γ rays obtained with inelastic contour for (a) Te^{44+}, (b) Te^{45+}, (c) Te^{46+}, and (d) Te^{47+}. (e) Simulated spectra of IC x rays and γ rays using (e) $\alpha_K^{44+}=10.8$ for Te^{44+}, (f) $\alpha_K^{45+}=13$ for Te^{45+}, (g) $\alpha_K^{46+}=4.7$ for Te^{46+}, (h) $\alpha_K^{47+}=0.3$ for Te^{47+}. See text for details.

treated simultaneously when determining the ρ versus $T_{1/2}$ curve. We assumed an $\alpha_K^{43}=10.9$ value equal to the theoretical coefficient [4]. From the experimental ρ^{44} value we obtained $T_{1/2}^{44} \leqslant 2$ ns and $\alpha_K^{44} \geqslant 8$. This value of α_K^{44} is in agreement, within experimental errors bars, with the theoretical value 10.8 calculated for normal IC. In the following analysis we shall adopt $\alpha_K^{44}=10.8$ and $T_{1/2}^{44}=1.6$ ns, corresponding to the calculated values [4].

Te^{45+}. The spectrum in Fig. 4(b) is conditioned by Te ions detected in the $Q=45$ charge state. The main characteristic of the spectrum is the very intense peak at 24 keV and the large ratio between the x-ray and γ-ray intensities. Te ions with $Q=45$ can be either (i) Te ions produced in $Q=44$, which after decay by a usual, energetically allowed, IC are transformed to $Q=45$ or (ii) Te ions exiting from the target with $Q=45$ which remain in this charge state after a BIC process or after emission of a γ ray. Under the present experimental conditions these two processes cannot be distinguished.

In the simulation, the decay of Te^{44+} and Te^{45+} were considered simultaneously to obtain the curve ρ versus $T_{1/2}$ conditioned by the detected charge state $Q=45$. The contribution from the decay by internal conversion from Te^{44+} to the number N_{IC} used the theoretical charge state distribution of ions at the exit of the target and the values of α_K^{44} and $T_{1/2}^{44}$ given above. The simulated curve of ρ^{45} versus $T_{1/2}^{45}$ is shown in Fig. 5, together with the result of the χ^2 analysis of the experimental spectrum compared to the simulated photon spectra in the energy range 20 to 33 keV. This yields values $\alpha_K^{45}=13^{+6}_{-3.5}$ and $T_{1/2}^{45}=1.4^{+0.4}_{-0.4}$ ns. Due to the small proportion of ions arising from decay of state $Q=44$ in the $Q=45$ detected ions, the value of α_K^{45} is not very sensitive to

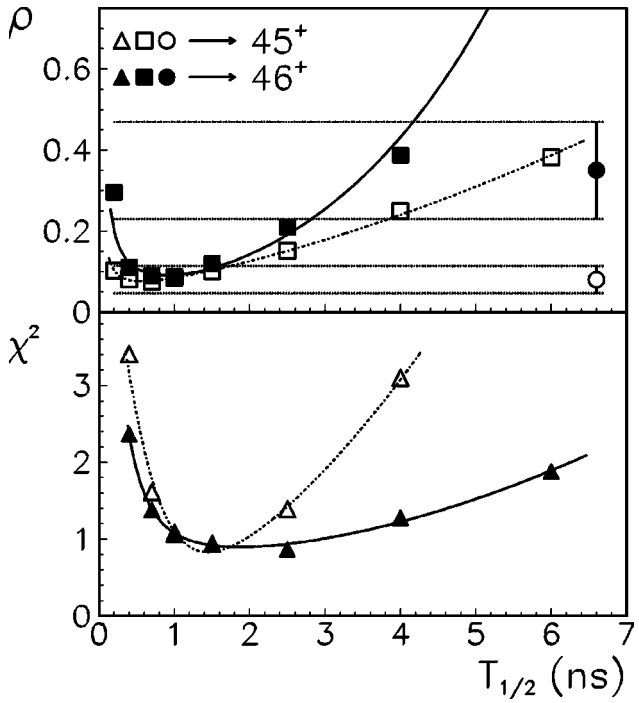

FIG. 5. Upper part: ρ versus $T_{1/2}$ obtained by simulating the decay of Te^{45+}, open squares, and Te^{46+}, filled squares. The curves are the results of a fit procedure, dotted-dashed curve for $Q=45$, full curve for $Q=46$. The open and filled circles are, respectively, the experimental ρ values with error bars for Te^{45+} and Te^{46+}. Lower part: reduced χ^2 between the experimental photon spectra and the simulated photon spectra for different $T_{1/2}$ values; $Q=45$ open triangles, dotted-dashed curve; $Q=46$ dark triangles, full curve.

the value taken for α_K^{44}. For example, $\alpha_K^{44}=15.6$ leads to a value $T_{1/2}^{45}=1.2$ ns.

The uncertainty in α_K^{45} is mainly due to the low intensity of the γ signal and to the subtraction of the elastic spectrum. The result is in quantitative agreement with the previous measurement of the half-life given in Ref. [2], where it was found that $T_{1/2}^{45}$ was at most equal to the value in neutral atom.

Te^{46+}. The photon spectrum in coincidence with Te ions in the 46^+ charge state is given in Fig. 4(c). In this case, *K*-shell IC can occur *only* by BIC. Therefore, the presence of Te *K* x rays at 24 keV emitted in flight is a definite proof of nuclear decay involving bound electrons in the initial and final states. Compared to the spectrum in Fig. 4(b), the ratio between N_{IC} and N_γ is very much reduced, indicating a smaller value of the IC coefficient as compared to $Q=45$. A diminution of α_K is expected as the density of states which can be occupied by the excited electron becomes lower. The analysis of this spectrum is simpler than for $Q=45$, because there is no mixing of different original charge states in coincidence with the photon signal. The curve ρ versus $T_{1/2}$ is shown in Fig. 5 together with the results of the χ^2 analysis. The curve of ρ versus $T_{1/2}$ indicates a value for $T_{1/2}$ between 2.8 ns and 4.0 ns whereas the minimum of the χ^2 curve favors a value for $T_{1/2}$ between 1 and 3.2 ns.

Te^{47+},Te^{48+}. The analysis of the spectrum in Fig. 4(d) shows that the IC coefficient for the *K* shell is even more reduced for the $Q=47$ charge state. The γ-ray peak dominates the photon spectrum and the emission of *K* x rays cannot be ascertained with the available statistics.

For $Q=48$ (not shown), we do not observe an x-ray signal. For this charge state, almost complete inhibition of BIC is expected, because the $2p$ shell of the Te ions is now completely empty. The latter fact has two consequences: (i) there is no electron left to fill the $1s$ shell except for an electron promoted to a high-lying bound state by internal conversion, (ii) the width of the $1s$ hole state becomes very small, so that the energy matching between the nuclear transition and an eventual atomic transition is very restricted.

In principle, the results of the simulation could be affected by long-lived metastable states. For the Te^{48+} ion, there is a well-known metastable configuration $1s^2 2p^2\,{}^3P_0$ with a lifetime of approximatively 1.7 ms [16,2]. The presence of ions in this state will not change the analysis because BIC transitions in such a state lie far from resonance and consequently such states cannot decay by BIC as is also the case for Te^{48+} ground state. For Te^{45+},Te^{46+}, and Te^{47+} if we restrict ourselves to configurations excited within the *L* shell, there are no metastable states with lifetimes longer than those taken into account in the theoretical analysis discussed below [18]. Metastable states formed with electrons in the *M* or higher shells will lie far from the resonance condition and consequently have negligible BIC decay rates.

Table I summarizes the results of the α_K and $T_{1/2}$ values obtained from the simulations for the different charge states of Te, together with the $T_{1/2}$ values measured previously [1,2]. Considering the difficulties associated with both the present method and that used previously, one recognizes general agreement between the two sets of experimental values.

CALCULATION OF BOUND INTERNAL CONVERSION

The results of theoretical calculations of BIC decay in ^{125}Te ion were presented in Ref. [4] and the values for the theoretical *K*-shell internal conversion coefficients are shown in Table I. The values for the ions $Q=45$ and $Q=46$ are significantly different from both sets of experimental results. One possible explanation of this difference is that the simplified atomic structure of Te ions considered in Ref. [4] led to the omission of resonant BIC transitions. In particular, the calculation of Ref. [4] considered the initial state ion Te $1s^2 2s^2 2\overline{p^2} 2p^{46-Q}$ to be in a single atomic state with the maximum number of electrons in $2\overline{p}$ orbitals. Here and below we use the notation $2\overline{p}$ to denote a $2pj=1/2$ orbital and the notation $2p$ to denote a $2pj=3/2$ orbital. Calculations [7] of excited atomic radiative decay rates of ionic states of the form Te $1s^2 2s^2 2\overline{p^x} 2p^y$ with $x\neq 2$ have revealed that such states have lifetimes of the order of nanoseconds or longer. These are comparable with, or longer than, the time during which IC x rays and γ rays are measured in the present experiment. This has the important consequence that

the number of possible BIC resonances is substantially increased relative to the case in which the $2p_{1/2}$ shell has the maximum occupancy.

Below we present the results of calculations of BIC decay in the ions Te^{45+} and Te^{46+} taking into account excited initial states. Details of these calculations are given in Ref. [7]. For both of these ionic states, the different possible distributions of electrons in $2\overline{p}$ and $2p$ orbitals give rise to five atomic states. The total rate for nuclear decay of a Te isomeric nuclear state for an ion in a given initial atomic state i can be written

$$\lambda_i = \sum_f \lambda_{if}^{\mathrm{BIC}} + \lambda^{\mathrm{IC}} + \lambda_\gamma, \tag{3}$$

where $\lambda_{if}^{\mathrm{BIC}}$ is the BIC decay rate to the final atomic state f, λ_γ is the radiative nuclear decay rate, and λ^{IC} is the rate for internal conversion decay to continuum states, which in the ions under consideration is limited by energy conservation to L-shell conversion.

The BIC decay rate is strongly dependent on the electronic transition energy as shown by the expression for the BIC coefficient α_{if} [4]

$$\alpha_{if} = \frac{\lambda_{if}^{\mathrm{BIC}}}{\lambda_\gamma} = \frac{A_{if}}{2\pi} \frac{\Gamma_{if}}{(\omega_\gamma - \omega_{if})^2 + \Gamma_{if}^2/4}, \tag{4}$$

where ω_γ is the nuclear transition energy, ω_{if} the atomic transition energy, and the quantity A_{if} (corresponding to $\alpha_{n\kappa}$ in Ref. [4]) is given by the same expression as that for the internal conversion coefficient to continuum states except that the wave function for the continuum electron, normalized on the energy scale, is replaced by that for a bound final state orbital. The quantity Γ_{if} in Eq. (4) is the total transition width which is dominated by the width ($\sim$ eV) of the $1s$ hole in the final state following excitation of a $1s$ electron by BIC. For the $M1$ transition of ^{125m}Te we have considered final states of the form $1s^1 2s^2 2\overline{p^x} 2p^y \mathrm{ns}^1$, created by $1s \rightarrow \mathrm{ns}$ BIC transitions. Such states are likely to be dominant since the electronic matrix elements are maximal for s orbital transitions. Additional contributions from $1s \rightarrow d_{3/2}$ transitions are possible but are associated with substantially smaller electronic matrix elements. The coupling between the open shell electrons in the final states considered leads to 19 different levels for Te^{45+} and 16 levels for Te^{46+}.

An example of $1s \rightarrow 8s$ BIC transitions in Te^{46+} is shown in Table II for those transitions lying within 80 eV of exact resonance. The transition energies, widths and A_{if} values have been calculated using Dirac-Fock electron wave functions calculated with GRASP [19]. In the calculations, the Auger contribution to the hole width and the effet of hyperfine interaction have been neglected. Very close energy matching between the electronic and nuclear transitions occurs for two electronic transitions of the excited state $1s^2 2s^2 2p^2 \ J=2$. The transition that is closest to resonance in the ground state $1s^2 2s^2 2\overline{p^2} \ J=0$ has an energy mismatch of 77 eV and thus lies relatively far from resonance, bearing in mind the magnitude ($\sim$eV) of the transition widths. In order to make the link with experiment, we have calculated the ratio $\rho^Q = N_\gamma / N_X$ assuming an initial statistical distribution of the five initial levels, taking account of the population and decay by atomic radiative transitions. After summing over all final levels with $n=8-20$ for Te^{45+} and $n=6-11$ for Te^{46+} we obtain $\rho^{45}=0.14$ and $\rho^{46}=0.41$. The experimental ρ values are, respectively, equal to $\rho^{45}=0.08\pm0.04$ and $\rho^{46}=0.35\pm0.12$. The good agreement between these values and the experimental data given above confirms the importance of BIC resonances in excited initial states.

TABLE II. Transitions energies and BIC coefficients α_{if} associated with the excitation $1s \rightarrow 8s$ in Te^{46+} for transitions with a resonance defect $|\omega_\gamma - \omega_{if}| < 80$ eV.

Initial state i	Final state f	$\omega_\gamma - \omega_{if}$ (eV)	α_{if}
$1s^2 2s^2 2\overline{p^1} 2p^2 \ J=0$	$1s^1 2s^2 2\overline{p^2} 8s^1 \ J=1$	-77.51	0.09
$1s^2 2s^2 2\overline{p^1} 2p^2 \ J=1$	$1s^1 2s^2 2\overline{p^2} 8s^1 \ J=0$	-76.58	0.05
$1s^2 2s^2 2\overline{p^1} 2p^1 \ J=1$	$1s^1 2s^2 2\overline{p^1} 2p^1 8s^1 \ J=2$	-63.75	0.07
$1s^2 2s^2 2\overline{p^1} 2p^1 \ J=1$	$1s^1 2s^2 2\overline{p^1} 2p^1 8s^1 \ J=0$	-62.95	0.04
$1s^2 2s^2 2\overline{p^1} 2p^1 \ J=1$	$1s^1 2s^2 2\overline{p^1} 2p^1 8s^1 \ J=0$	-32.11	0.62
$1s^2 2s^2 2\overline{p^1} 2p^1 \ J=1$	$1s^1 2s^2 2\overline{p^1} 2p^1 8s^1 \ J=1$	-31.98	1.19
$1s^2 2s^2 2\overline{p^1} 2p^1 \ J=2$	$1s^1 2s^2 2\overline{p^1} 2p^1 8s^1 \ J=3$	-66.25	0.06
$1s^2 2s^2 2\overline{p^1} 2p^1 \ J=2$	$1s^1 2s^2 2\overline{p^1} 2p^1 8s^1 \ J=2$	-66.56	0.04
$1s^2 2s^2 2\overline{p^1} 2p^1 \ J=2$	$1s^1 2s^2 2\overline{p^1} 2p^1 8s^1 \ J=1$	-31.55	0.34
$1s^2 2s^2 2\overline{p^1} 2p^1 \ J=2$	$1s^1 2s^2 2\overline{p^1} 2p^1 8s^1 \ J=2$	-31.33	0.51
$1s^2 2s^2 2p^2 \ J=2$	$1s^1 2s^2 2p^2 8s^1 \ J=3$	-43.88	0.08
$1s^2 2s^2 2p^2 \ J=2$	$1s^1 2s^2 2p^2 8s^1 \ J=2$	-43.13	0.07
$1s^2 2s^2 2p^2 \ J=2$	$1s^1 2s^2 2p^2 8s^1 \ J=1$	-4.26	16.39
$1s^2 2s^2 2p^2 \ J=2$	$1s^1 2s^2 2p^2 8s^1 \ J=2$	-4.13	25.65
$1s^2 2s^2 2p^2 \ J=0$	$1s^1 2s^2 2p^2 8s^1 \ J=1$	-28.23	0.81

CONCLUSION

We have directly measured the ratio of K x rays to γ rays following internal conversion in ^{125}Te ions with charge states ranging between 44^+ and 48^+. For charge states $Q=45^+$ and, especially, $Q=46^+$, a clear K_α x-ray signal was obtained, which proves without ambiguity the presence of IC in a situation where the K-shell electron binding energy is larger than the nuclear transition energy. The K_α x-ray signal disappears for Te ions with $Q=48^+$.

The measured values of the nuclear lifetimes for $Q=45^+$ to $Q=48^+$ Te are in general agreement with the values previously measured by a different method. For the charge states $Q=45^+$, $Q=46^+$, good agreement between the experimental data and the theoretical calculations is obtained if excited configurations of $2p$ electrons are considered. This splits a given $1s$ to ns transition into different branches with different energies. Additional splittings arise from coupling between electrons in different open shells. The net result is that a rich resonance structure is produced which leads to an enhancement of the nuclear decay probability. In this situation it is no longer possible to define a unique internal conversion coefficient or a single lifetime for

an ion in a given charge state. Instead the full electronic configuration should be considered in the definition of the BIC coefficient.

It is interesting to note that the BIC process is exactly the reverse process of NEET in which the nucleus is excited by a near-resonant electronic transition [17]. If we assume a prepared excited atomic state which can decay by a transition whose approximate energy matches a nuclear transition in the same atom, it is possible for the excitation energy of the electronic part of the atom to be transfered to the nuclear part of the atom. The matrix elements coupling the electronic and nuclear currents are exactly the same in BIC and in NEET if the electronic and nuclear states involved in BIC and NEET are identical. In order to observe the NEET process corresponding to the BIC decay of ^{125}Te observed here, one would have to prepare a ^{125}Te ion in the electronic configuration $1s^1 2s^2 2p^3 ns^1$ (with $n \sim 17$) or in the configuration $1s^1 2s^2 2p^2 ns^1$ (with n equal 8 or 9), which is obviously very difficult. Nevertheless suitable situations for the observation of BIC might be encountered in other atoms. In particular, one favorable system may be the case of ^{235}U excited electronically in a laser-heated plasma [20].

[1] F. Attallah, M. Aiche, J.F. Chemin, J.N. Scheurer, W.E. Meyerhof, J.P. Grandin, P. Aguer, G. Bogaert, C. Grunber, J. Kiener, A. Lefebvre, and J.P. Thibaud, Phys. Rev. Lett. **75**, 1715 (1995).

[2] F. Attallah, M. Aiche, J.F. Chemin, J.N. Scheurer, W.E. Meyerhof, J.P. Grandin, P. Aguer, G. Bogaert, C. Grunber, J. Kiener, A. Lefebvre, and J.P. Thibaud, Physica C **55**, 1665 (1997)

[3] M. Breining, M.H. Chen, G.E. Ice, F. Parente, and B. Crasemann, Phys. Rev. A **22**, 520 (1980).

[4] F. Bosch, T. Faestermann, J. Friese, F. Heine, P. Kienle, E. Zeitelhack, K. Beckert, B. Franzke, O. Keppler, C. Kozhuharov, G. Menzel, R. Moshammer, F. Nolden, H. Reich, B. Schlitt, M. Steck, T. Stöhlker, T. Winkler, and K. Takahashi, Phys. Rev. Lett. **77**, 5190 (1996).

[5] K. Takahashi and K. Yokoi, At. Data Nucl. Data Tables **36**, 375 (1987).

[6] F.F Karpeshin, M.R. Harston, F. Attallah, J.F. Chemin, J.N. Scheurer, I.M. Band, and M.B. Trzhaskovskaya, Phys. Rev. C **53**, 1640 (1996).

[7] M.R. Harston, T. Carreyre, and J. F. Chemin, Nucl. Phys. **A676**, 143 (2000).

[8] L. Bianchi, B. Fernandez, J. Gastebois, A. Gillibert, W. Mittig, and J. Barrette, Nucl. Instrum. Methods Phys. Res. A **276**, 509 (1989).

[9] W.E. Meyerhof and K. Taulberg, Annu. Rev. Nucl. Sci. **27**, 279 (1977).

[10] R. Anholt, H.H. Behncke, S. Hagmann, P. Armbruster, F. Folkmann, and P.K. Mokler, Z. Phys. A **289**, 349 (1979).

[11] S.I. Salem and L.E. Lee, At. Data Nucl. Data Tables **18**, 253 (1976).

[12] F. Attallah, Ph.D. thesis, University of Bordeaux I, 1994.

[13] M. Goosens, ''GEANT: Detector Description and Simulation Tool,'' CERN program library long write-up, 1993 (unpublished).

[14] *Table of Isotopes*, edited by R. B. Firestone *et al.*, 8th ed. (Wiley-Interscience, New York 1996) Vol II F56.

[15] W.R. Phillips, K.E. Rehm, W. Henning, I. Ahmad, J.P. Schiffer, B. Glagola, and T.F. Wang, J. Phys. (France) **48**, C9-311 (1987).

[16] J.P. Marques, F. Parente, and P. Indelicato, Phys. Rev. A **47**, 929 (1993).

[17] M. Morita, Prog. Theor. Phys. **41**, 1574 (1973).

[18] K.T. Cheng Y.K. Kim, and J.P. Desclaux, At. Data Nucl. Data Tables **24**, 111 (1979).

[19] I.P. Grant, B.J. McKenzie, P.H. Norrington, D.F. Mayers, and N.C. Pyper, Comput. Phys. Commun. **21**, 207 (1980).

[20] M.R. Harston and J.F. Chemin, Phys. Rev. C **59**, 2462 (1999).